Environ Earth Sci (2017) 76:125
DOI 10.1007/s12665-017-6444-9

ORIGINAL ARTICLE

Mapping and detection of land use change in a coal mining area using object-based image analysis

Wenming Pei[1] · Suping Yao[1] · Joseph F. Knight[2] · Shaochun Dong[3] · Keith Pelletier[2] · Lian P. Rampi[2] · Yan Wang[2] · Jim Klassen[2]

Received: 6 January 2016 / Accepted: 24 January 2017 / Published online: 3 February 2017

Abstract Object-based image analysis was used to map land use in the Panxie coal mining area, East China, where long-term underground coal mines have been exploited since the 1980s. A rule-based classification approach was developed for a Pleiades image to identify the desired land use classes, and the same rule-based classification strategies, after the threshold values had been modified slightly, were applied to the Landsat series images. Five land use classes were successfully captured with overall accuracies of between 80 and 94%. The classification approach was validated for its flexibility and robustness. Multitemporal classification results indicated that land use changed considerably in the Panxie coal mining area from 1989 to 2013. The urban, coal and coal gangue, and water areas increased rapidly in line with the growth in mine production. Urban areas increased from 9.38 to 20.92% and showed a tendency to increase around the coal mines. From 1989 to 2013 the coal and coal gangue area increased by 40-fold, from 0.02 to 0.58%. Similarly, the water area increased from 2.77 to 7.84% over this time period, mainly attributable to the spread of waterlogged areas. The waterlogged areas increased to about 2900 ha in 2013, which was about 80 times more than their area in 1989. In contrast, the area of cultivated land was negatively related to the increase in mine production and decreased from 73.11 to 57.25%. The results of this study provide a valuable basis for sustainable land management and environmental planning in the Panxie coal mining area.

Keywords Coal mining area · Land subsidence · Land use change · Object-based image analysis (OBIA) · Waterlogged area

✉ Suping Yao
spyao@nju.edu.cn

Wenming Pei
wenmpei@gmail.com

Joseph F. Knight
jknight@umn.edu

Shaochun Dong
dsc@nju.edu.cn

Keith Pelletier
keith.pelletier@gmail.com

Lian P. Rampi
ortiz073@umn.edu

Yan Wang
wang3606@umn.edu

Jim Klassen
klassen.js@gmail.com

[1] MOE Key Laboratory of Surficial Geochemistry, School of Earth Sciences and Engineering, Nanjing University, 163 Xianlin Ave, Nanjing 210023, China

[2] Department of Forest Resources, University of Minnesota, 1530 Cleveland Ave N, St. Paul, MN 55108, USA

[3] School of Earth Sciences and Engineering, Nanjing University, 163 Xianlin Ave, Nanjing 210023, China

Introduction

Extensive exploitation of underground coal mines results in land subsidence, which can impact biological diversity, contribute to forest fragmentation, lead to land use change, alter ecosystem services, disrupt socio-cultural practices, and increase the risk of geohazards such as flooding, soil erosion, and ground fissures (Vitousek et al. 1997; Townsend et al. 2009; Jiao et al. 2012). This situation is particularly common in East China, an important region for coal mining and agricultural production. Most coal mining

areas in East China are close to densely populated towns and small cities. In areas of long-term underground coal mining activities, particular land use types develop, cultivated lands are degraded, and seasonally or perennially waterlogged areas form because of the shallow groundwater table level; these environmental changes in turn restrict regional economic development, intensify the tension between people and land use, and lead to a series of social problems (Hu and Zhao 2007; Hu et al. 2012). Therefore, accurate and dynamic monitoring of land use change in coal mining areas is urgently needed and is important for the sustainable use of land resources, for social stability, and for environmental protection (Ma and Liu 2011).

Remote sensing has become an important tool for monitoring dynamic changes in natural resources and the environment (Zhao 2003; Chen et al. 2009; Feyisa et al. 2014); it can be used at a range of scales, including the macroscale, and the same image can be used for a range of analyses. Remote sensing has been widely used to characterize spatial and temporal land use changes, including the spread of urbanization (Jensen 1981; Yang and Lo 2002), and changes in the extent of surface water resources (Sheng and Kuang 2003; Rawashdeh et al. 2013) and natural vegetation cover (Thenkabail et al. 2004; Wardlow et al. 2007). Many previous studies have applied remote sensing techniques to detect land use change in coal mining areas (Du et al. 2007; Gao et al. 2009). In most of these studies, land use was mapped by extracting information from remotely sensed datasets using traditional pixel-based classification techniques (Prakash and Gupta 1998; Townsend et al. 2009; Bian and Lu 2013). These techniques only use spectral information in the image classification procedure and may produce acceptable results with moderate-resolution imagery; however, they cannot solve the problems of high spectral variation within classes and spectral similarity between classes that occur when high-resolution imagery is used (Cleve et al. 2008). For example, cultivated lands and grasslands, and cement roads and coal gangue piles exhibit similar spectral responses and so are prone to misclassification. Hence, there are still challenges associated with accurate classification of land use in coal mining areas using spectral information only.

Recently, as higher-resolution spatial data have become available, object-based image analysis (OBIA) has been accepted as an efficient method for analyzing remote sensing data (Blaschke 2010; Belgiu et al. 2014). This method is considered as a new and evolving paradigm in remote sensing (Blaschke et al. 2014). As an iterative image analysis method, OBIA starts by using image segmentation to partition the image into homogeneous image objects (Baatz and Schäpe 2000). Once the image objects are generated, a large number of image object features can be computed and used in the subsequent classification task (Belgiu et al. 2014). In contrast to traditional pixel-based analysis, OBIA incorporates not only spectral data, but also textural, spatial, and contextual information. To classify the image objects, the image operators have to determine the most relevant features and their corresponding thresholds from a large number of available image features. Spectral and spatial information can be combined within OBIA to extract land use objects (Kindu et al. 2013). For example, previous studies have successfully used OBIA with medium- and high-resolution imagery to extract urban objects (Chen et al. 2007; Xu 2013), delineate tree crowns (Bunting and Lucas 2006), and map wetlands (Moffett and Gorelick 2013). Du et al. (2007) compared traditional and object-oriented classification methods in monitoring land use change in the Xuzhou coal mining area using Landsat TM/ETM+ and ASTER data and found that the object-based classification method was suitable for the truth categories. To date, image classification using the object-based approach has not been tested in studies of land use change in underground coal mining areas, even though many researchers agree that such studies should be prioritized (Bian and Zhang 2006; Du et al. 2007; Yu et al. 2015). Timely and accurate information about land use change is not only helpful for understanding past and present land use, but can also ensure compliance with environmental regulations or permitting in coal mining areas.

The overall objective of this study was to investigate the feasibility and accuracy of applying the OBIA classification approach to images of different spatial resolution and to map long-term land use changes in underground coal mining areas. The specific objectives were to (1) develop the object-based classification approach to extract land use information from high-resolution imagery data in underground coal mining areas; (2) evaluate the effectiveness of the developed OBIA method using multitemporal Landsat images, and (3) understand how land use in underground coal mining areas changes over time as a consequence of continued underground coal mining.

Materials and methods

Study area

The study area, the Panxie coal mining area, is located in Huainan City, Anhui Province, East China, near the Huaihe River. It covers an area of approximately 62,000 ha, from 32°43′ to 32°56′N, and from 116°22′ to 116°57′E (Fig. 1). The study area has a shallow groundwater table and is relatively flat with an average elevation of between 30 and 40 m above sea level (Dong et al. 2013). Coal seams have

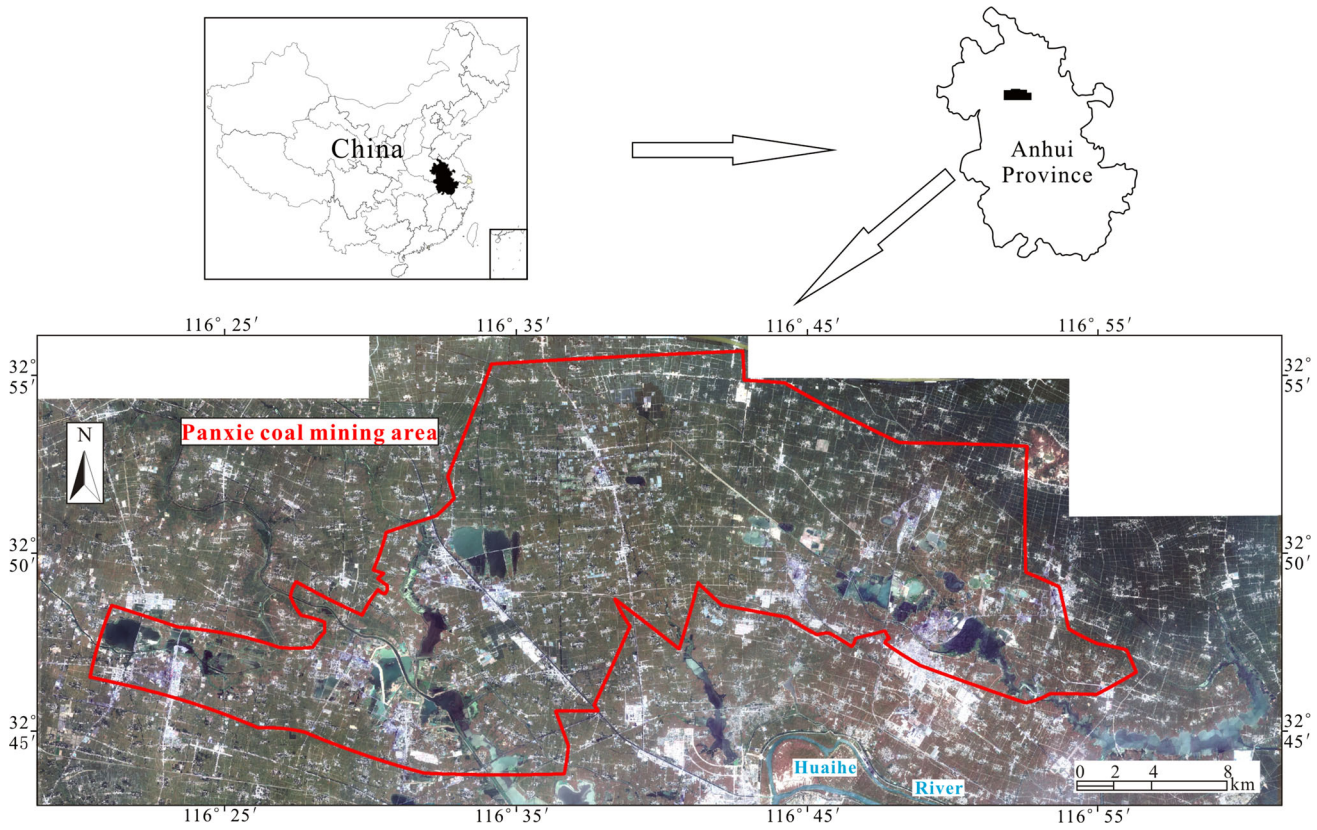

Fig. 1 Location of the study area in Anhui Province, China. The Panxie coal mining area is indicated by the red thick red line (image provided by the Huainan Mining Industry Group)

been mined extensively in the area since the 1980s, and the produced coal has fueled the economic development of East China over the last 30 years. However, this area has experienced dynamic changes in land use because of the long-term extensive underground coal mining activities, including large-scale land subsidence and the formation of large areas of seasonally and perennially waterlogged areas. Consequently, in such areas the surface structures, buildings, farmlands, and man-made drainage systems have been destroyed (Dong et al. 2013), as shown in Fig. 2. Therefore, ecosystems in the study area have become increasingly vulnerable and are a major concern for local government, the mining industry, and environment groups.

Data acquisition

Two types of remote sensing images, Pleiades and Landsat, with different spatial resolutions were used to map the land use in this study. The Pleiades images had a spatial resolution of 2.0 m in multispectral mode (three visible bands and one near-infrared band) and a pixel size of 0.5 m in panchromatic mode, and were acquired on April 30, 2013. Multitemporal images from the Landsat series of satellites have been used for land use mapping and change detection many times in the past (Jensen 1981; Townsend et al. 2009; Hu et al. 2012). We acquired six cloud-free Landsat images for 1989, 1998, 2003, 2007, 2009, and 2013 that covered the entire study region for the maximum time period possible from the beginning of coal mine activity (Table 1). The Pleiades and Landsat images were from approximately the same time of year, so seasonal variations in water level and vegetation cover were eliminated.

Data pre-processing

The Pleiades images were geometrically corrected with Registration Control Point (RCP) files from the Pleiades satellite and resampled using the nearest-neighbor method. The multitemporal Landsat images were corrected using the image-to-image method in ERDAS Imagine 2013, using the Pleiades images as a reference. To ensure consistency between datasets during analysis, all data were projected to the Universal Transverse Mercator projection system (zone 50 N) and the World Geodetic System 84 datum. The images were clipped to show only the Panxie coal mining area using shapefile data provided by the Huainan Mining Industry (Group).

Fig. 2 Examples of **a** cultivated land and **b** urban area submerged by water in the Panxie coal mining area

Image classification methods

In this study, five typical land use classes were mapped in the Panxie coal mining area: cultivated land, urban area, grassland and woods, coal and coal gangue, and water (Table 2). To reduce the time needed to classify the high-resolution imagery (Pleiades images), a small subset (6000 × 5000 pixels) of the study area that contained typical land use classes was used to develop the classification approach. Using a trial-and-error process, we selected and applied the best classification rulesets and thresholds of the features to the rest of the high-resolution imagery. The OBIA classification approach was implemented in the Trimble eCognition Developer software package (Trimble 2013).

Instead of operating directly on single pixels, OBIA works on objects with many pixels that have been grouped together into image objects by image segmentation to avoid the salt–pepper effect (Desclée et al. 2006; Huang et al. 2014). Image segmentation is a key preliminary step in OBIA that divides the image into homogeneous, contiguous, and meaningful objects. We used a multiresolution segmentation algorithm based on the Fractal Net Evolution Approach (FNEA) (Baatz and Schäpe 2000). The algorithm starts with single image objects of one pixel and repeatedly merges them into pairs in several loops to form larger units as long as an upper threshold of homogeneity is not exceeded locally (Thapa et al. 2014). There are three key parameters in an image, namely shape, compactness, and the scale, for either object segmentation or pixels that have similar spectral and spatial signatures. The settings of the segmentation parameters are determined by several factors, such as the data type, the nature of the study area, and the range of land use classes (Espindola et al. 2006). The shape and compactness parameters range from 0 to 1 and can determine objects at different scales and control the homogeneity of objects. In this study, the shape parameter was set to 0.3 to give less weight to shape and to give more attention to the spectral homogeneity of objects for segmentation. The compactness parameter was set to 0.5 to balance the compactness and smoothness of the objects equally. The scale parameter that controls the object size is the most important parameter of image segmentation. In this study, the optimal scale parameters of the images with different resolution were selected after careful examination of the spatial patterns (Table 3). For the Pleiades images, the scale parameter was set to 20 for the 'cultivated land' and 'water' classes and to 15 for the 'urban area,' 'grassland and woods,' and 'coal and coal gangue' classes. For the Landsat-8, Landsat-7, and Landsat-5 images, the scale parameter was set to 20, 10, and 5, respectively. It is important to note that there is no

Table 1 Main features of the remote sensing images

Satellite	Sensor	Acquisition date	Spatial resolution (m)
Pleiades	E2 V	April 30, 2013	Multispectral bands: 2/Panchromatic band: 0.5
Landsat-8	OLI	April 28, 2013	Multispectral bands: 30/Panchromatic band: 15
Landsat-7	ETM^{+}	April 16, 2003	Multispectral bands: 30/Panchromatic band: 15
Landsat-5	TM	April 8, 2009	Multispectral bands: 30
Landsat-5	TM	April 19, 2007	Multispectral bands: 30
Landsat-5	TM	May 28, 1998	Multispectral bands: 30
Landsat-5	TM	April 26, 1989	Multispectral bands: 30

Table 2 Land use classification scheme

Land use type	Description
Cultivated land	Agricultural area, crop fields
Urban area	Residential, commercial and services, industrial, transportation, roads
Grassland and woods	Grass, scrub, trees, and others
Water	River, lakes, ponds, and waterlogged areas
Coal and coal gangue	Coal piles and coal gangue piles

Table 3 Segmentation parameters of the various images

Image	Scale parameter	Shape	Compactness
Pleiades	15 (urban area; grassland and woods; coal and coal gangue)/20 (cultivated land; water)	0.3	0.5
Landsat-8	20	0.3	0.5
Landsat-7	10	0.3	0.5
Landsat-5	5	0.3	0.5

standardized or optimal scale for different kinds of remotely sensed images (Myint et al. 2011).

After the objects were formed, a rule-based classification approach was applied to identify the desired land use classes from the image. In this study, a two-level classification hierarchy was created: Vegetated and non-vegetated areas were defined on the first hierarchy level. Subsequently, the 'cultivated land' and 'grassland and woods' classes were defined as a subclass of the vegetation class, and the other classes were defined as subclasses of the non-vegetated class. The classification rulesets define the membership of the image objects to a given class by a set of fuzzy or crisp membership functions (Zhou et al. 2014a, b). The user's expert knowledge can be used to define the rules and constraints in the membership function that control the classification procedure. A large set of features can be calculated for each object operating in the semantic hierarchy to provide comprehensive information about its spectral, textural, spatial, and contextual properties (Baatz and Schäpe 2000; Chen et al. 2007), especially in images with high spatial resolution. It is particularly important to incorporate spatial and textural information with spectral information in land use classification, since different land use classes with similar spectral properties may have distinct spatial characteristics (e.g., the 'cultivated land' class and the 'grassland and woods' class, and the 'coal and coal gangue' class and the 'urban area' class).

Vegetation areas were masked out using the Fuzzy-Range-Function of the Normalized Difference Vegetation Index (NDVI). The NDVI was calculated using the near-infrared (NIR) and red bands as follows:

$$\mathrm{NDVI} = \frac{\mathrm{NIR} - \mathrm{Red}}{\mathrm{NIR} + \mathrm{Red}} \tag{1}$$

To discriminate the 'cultivated land' class and the 'grassland and woods' class from the vegetated areas, shape and texture features were used, including shape values of rectangular fit (RECF) and area, and the texture value of the gray-level co-occurrence matrix (GLCM) homogeneity (Haralick 1979). The RECF and area values of these two classes are distinct. The cultivated lands are regularly shaped, while grassland and woods have more complex boundaries (Jiao et al. 2012). Moreover, GLCM homogeneity indicates the homogeneity of an object based on the gray-level co-occurrence matrix. Cultivated lands have relatively large values for the GLCM homogeneity texture.

$$\mathrm{RECF} = a/l_{\max} \times l_{\min} \tag{2}$$

where a is the area of the polygon and l is the length of the major/minor axis.

$$\mathrm{Homogeneity} = \sum_{i,j=0}^{N-1} P_{i,j} / \left\{1 + (i-j)^2\right\} \tag{3}$$

where i is the row number, j is the column number, and N is the number of rows or columns. The parameter $P_{i,j}$ calculated using Eq. (4) is the normalized value in cell i, j. $V_{i,j}$ is the value in the cell i, j of the GLCM (Shiraishi et al. 2014).

$$\mathrm{P}_{i,j} = V_{i,j} / \sum_{i,j=0}^{N-1} V_{i,j} \tag{4}$$

Water features were classified using a Fuzzy-Range-Function of the Normalized Difference Water Index (NDWI). This index has been successfully used to classify and extract water (Gao 1996; Xu 2006). Previous studies have shown that the water extraction may be improved

using other water indices, including the Water Index (Ouma and Tateishi 2006), Modified Normalized Difference Water Index (MacFeeters 1996), and Automated Water Extraction Index (Feyisa et al. 2014). However, these water indices were not used in this study because of the band limitations of the Pleiades images. The NDWI was calculated using the green and NIR bands as follows

$$\mathrm{NDWI} = \frac{\mathrm{Green} - \mathrm{NIR}}{\mathrm{Green} + \mathrm{NIR}} \quad (5)$$

The 'coal and coal gangue' class, a land use class that is unique to coal mining areas, is common near the mines in the study area. Crisp membership functions were used to identify this class using brightness, NDVI, and area. The brightness (B) was defined as the sum of the object means in the visible bands ($\bar{C}_i(\mathrm{vis})$) divided by the number of visible bands (n_{vis}) (Stumpf and Kerle 2011), as follows:

$$\mathrm{B} = \frac{1}{n_{\mathrm{vis}}} \sum_{i=1}^{n_{\mathrm{vis}}} \bar{C}_i(vis) \quad (6)$$

There is significant confusion between the signatures for this class and those of cement rooftops and roads because of the low brightness value. Thus, two shape features, such as length/width and rectangular fit, were used to identify the 'coal and coal gangue' class.

Shadows are present in all high-resolution images (Zhou et al. 2009). To avoid misclassification of shadows from buildings and to exclude vegetated areas near the buildings in the Pleiades image, a relative border to the 'grassland and woods' and the NDVI were applied to the 'grassland and woods' class.

The step-by-step procedures for obtaining high-resolution images of the study area are presented in Fig. 3, which also shows a subset of the original Pleiades image and the output map of the object-based approach.

The rule-based classification strategies that were developed to classify land use in the Panxie coal mining area were applied to the Landsat images after the threshold values were slightly modified. Fewer spatial and textural parameters (e.g., length/width and rectangular fit) were integrated into the rule-based land use classification process for the Landsat images than for the Pleiades images because of the coarse spatial resolution. The step-by-step procedure that was applied to the Landsat images in this study is presented in Fig. 4.

Accuracy assessment

Although object-based accuracy assessment has been used to demonstrate that the segmentation of objects at different scales is appropriate (Myint et al. 2011), it cannot reflect the actual classification accuracy or whether each image pixel has been accurately identified from the reference data. Thus, in this study we performed an accuracy assessment of the land use classification at the pixel level based on a subset of sample pixels that were assumed to represent the whole image. The OBIA classification result was assessed by the overall accuracy, Kappa coefficient, producer's accuracy, user's accuracy, and Kappa coefficient based on the traditional error matrix. The producer's and the user's accuracies were used to evaluate the omission and commission errors for each class. To obtain precise estimates of accuracy, a minimum of 50 points per class was set in a stratified random sampling approach (Stehman 2009; Foody 2011). To eliminate class-level bias, this method allocates the sample size for each land use class based on its spatial extent (Thapa et al. 2014). Reference information was collected from high-resolution images (Pleiades images) and Google Earth images. Because of data limitations, the high-resolution images (Pleiades images) were only used to assess the land use maps from 2013. The accuracies of the multitemporal classifications (1989, 1998, 2003, 2007, and 2009) were assessed using Landsat-5/7 images and historical images (October 2006, February 2008, May 2010) obtained from Google Earth.

Change detection

Statistical methods can be used to quantitatively analyze multitemporal land use change. Post-classification change analysis was used to minimize the possible effects of atmospheric variation and sensor differences (Lu et al. 2004). This analysis performs a per-pixel comparison between time periods in matrix form and the separately classified images for each time period (Peneva-Reed 2014). Images of different reference years were first independently classified. The classified images from 1989 to 2013 were compared. The change rates of each class were calculated using the following equation:

$$\mathrm{Landusechangerate} = \left(\frac{\mathrm{Area}_{\mathrm{final\ year}} - \mathrm{Area}_{\mathrm{initial\ year}}}{\mathrm{Area}_{\mathrm{initial\ year}}} \right) \times 100 \quad (7)$$

where Area is the extent of each land use type. Positive values suggest an increase in extent and vice versa. The conversion matrix, which summarizes all of the 'from–to' changes in land use classes, was used to analyze the change status and its driving mechanisms and trends (Moffett and Gorelick 2013; Peneva-Reed 2014). The land use conversion matrices for the time period from 1989 to 2013 were generated using ArcGIS 10 software and compiled in a matrix table, and the values are presented in hectares.

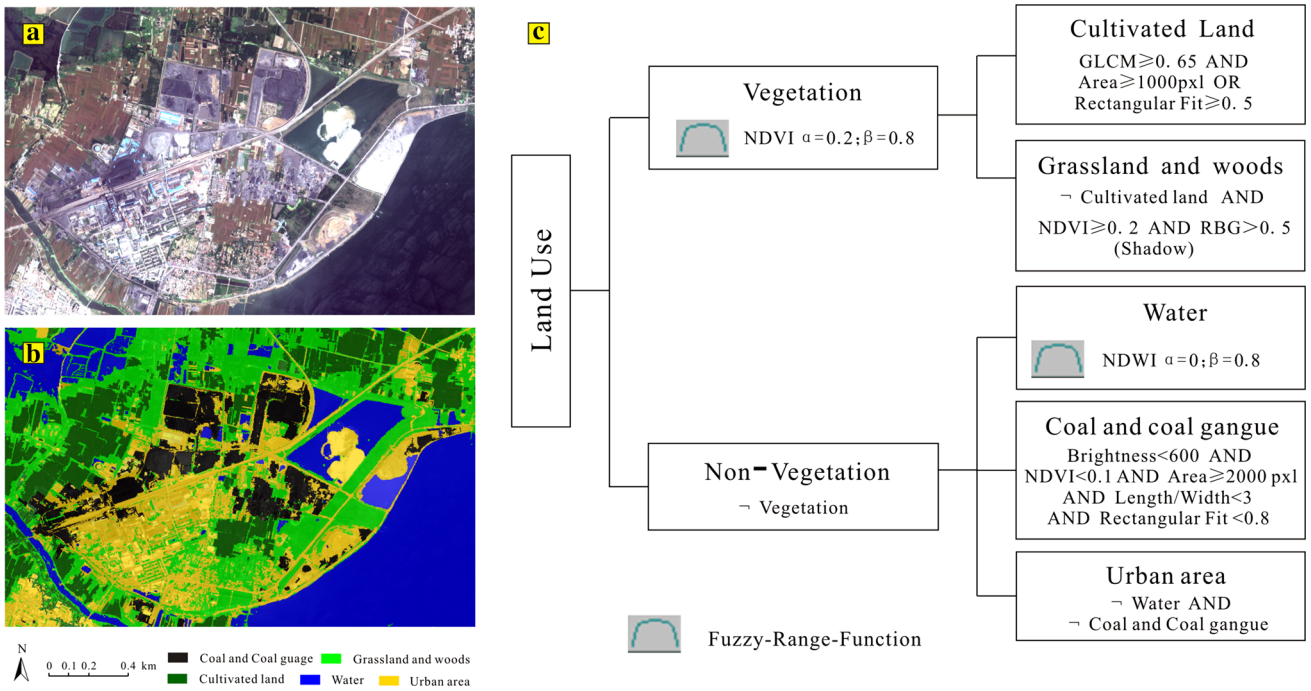

Fig. 3 Rule-based classification of the selected land use classes. **a** A subset of the original Pleiades image; **b** output map for the object-based approach; **c** rulesets. NDVI—Normalized Difference Vegetation Index; GLCM—gray-level co-occurrence matrix values; NDWI—Normalized Difference Water Index; RBG—relative border to 'grassland and woods'; α-lower border; β-upper border

Results

Classification and accuracy assessment results of the Pleiades data

The rule-based classification was applied to the study area in the Pleiades image using the same classification parameters that were defined for the small subset area. The classification results are shown in Fig. 5. Accuracy assessment results are summarized in Table 4. The classification results show that the OBIA classification approach produced a significantly higher overall accuracy (94%) and Kappa coefficient (0.92). All classes achieved a high producer's accuracy. The 'coal and coal gangue' class produced the lowest producer's and user's accuracies (91 and 87%, respectively). The 'water' class achieved the highest producer's and user's accuracies (97 and 97%, respectively). The second highest producer's and user's accuracies were obtained for the 'urban area' class (96 and 96%, respectively). The 'grassland and woods' class achieved relatively higher producer's and user's accuracies (92 and 97%, respectively). The 'cultivated land' class also achieved relatively higher producer's and user's accuracies (94 and 91%, respectively).

Classification and accuracy assessment results of the Landsat series data

The classification results are shown in Fig. 6, and the accuracy assessment of the Landsat-8 imagery for the same sampling points is summarized in Table 5. The overall accuracy (88%) and Kappa coefficient (0.86) from the OBIA classification of the Landsat-8 images were lower than for the high-resolution images for the same period. Of the five classes, the 'water' class was the most accurately classified, with a producer's accuracy of 89% and a user's accuracy of 97%. The 'grassland and woods' and 'coal and coal gangue' classes gave low producer's accuracy (86 and 82%, respectively) and user's accuracy (84 and 84%, respectively). The 'cultivated land' class achieved the highest producer's accuracy (95%) and the lowest user's accuracy (81%). In contrast, the 'urban area' achieved the highest user's accuracy (92%) but a somewhat lower producer's accuracy (85%). This is because of confusion between the 'grassland and woods' and 'cultivated land' classes and between the 'coal and coal gangue' and 'urban area' classes. These misclassifications mainly reflect the medium spatial resolution of the Landsat images, which combined spectral properties of heterogeneous land use classes in resolution cells (Lu et al. 2011).

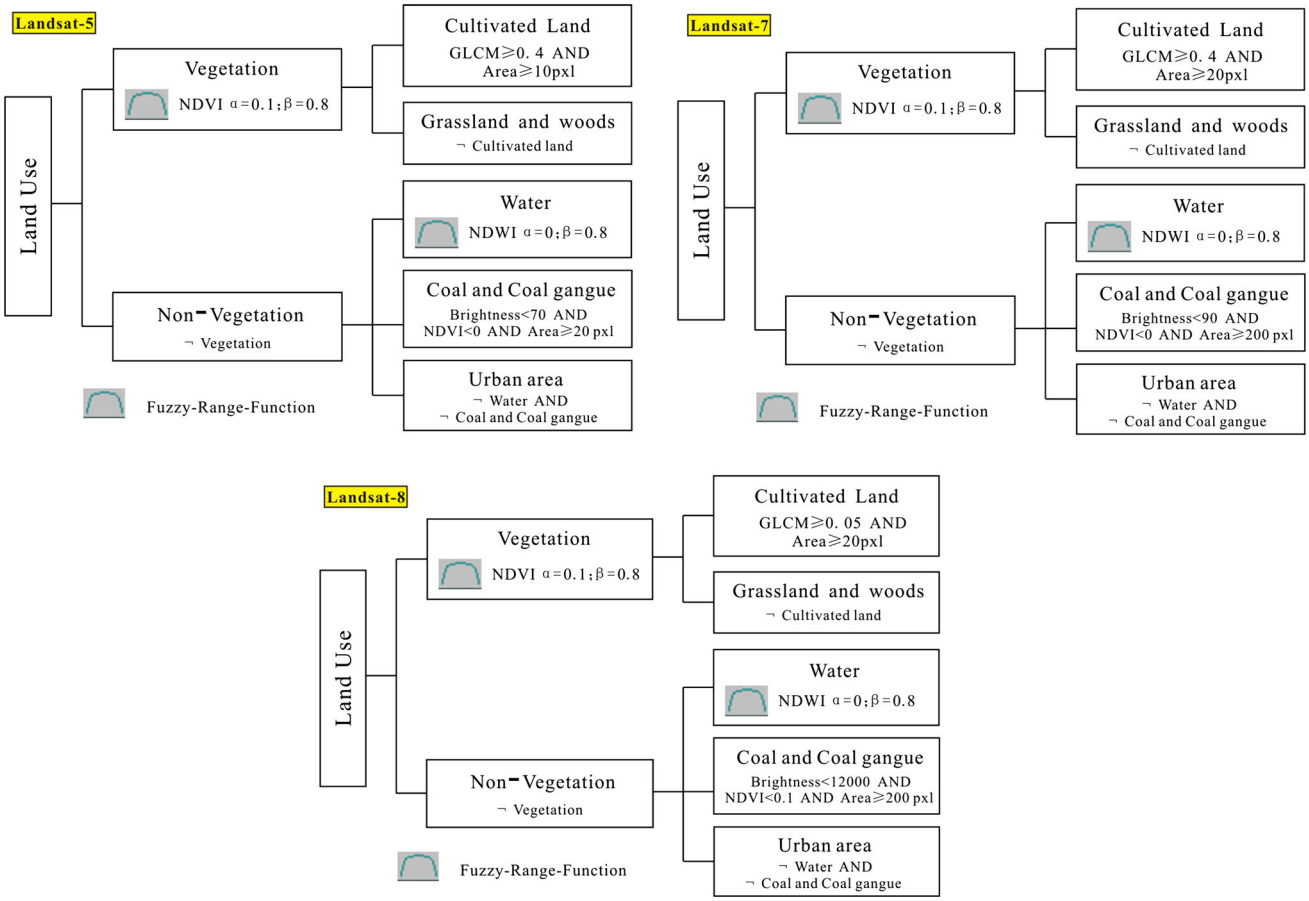

Fig. 4 Flowcharts used for analysis of Landsat-5, Landsat-7, and Landsat-8 images. NDVI-Normalized Difference Vegetation Index; GLCM-Gray-level co-occurrence matrix values; NDWI-Normalized Difference Water Index; α-lower border; β-upper border

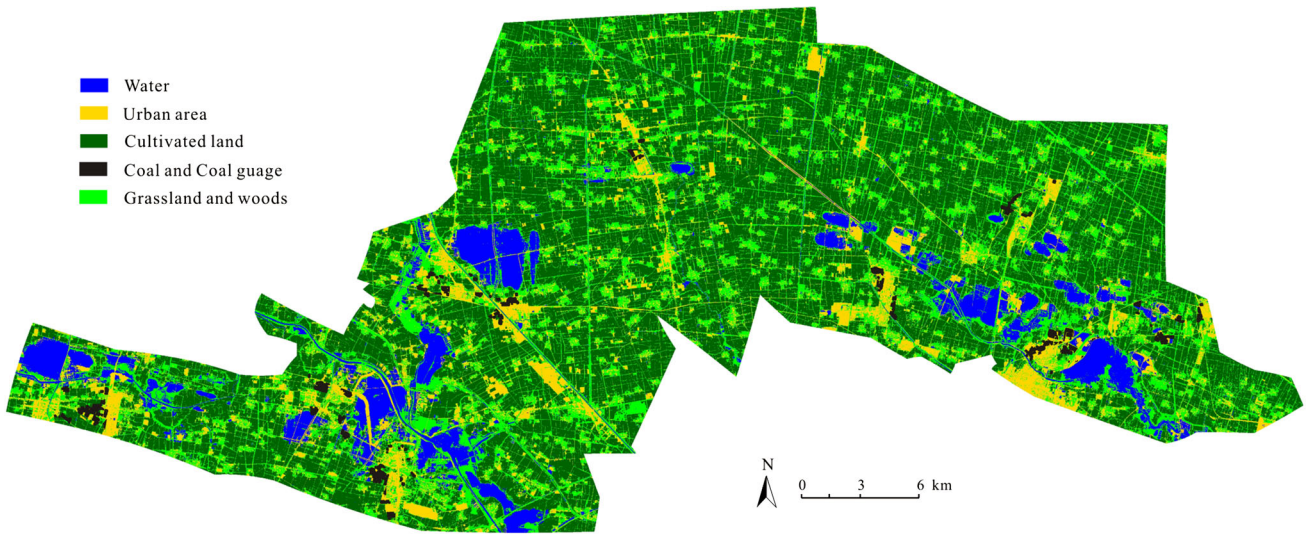

Fig. 5 Classification result from Pleiades imagery for 2013

The results of accuracy assessments of the Landsat-5 and Landsat-7 images are reported in Table 6. For the images obtained in 1989, 1998, 2003, 2007, and 2009, the accuracies (80, 82, 86, 84, and 85%, respectively) and Kappa coefficients (0.75, 0.79, 0.83, 0.81, and 0.84, respectively) are generally satisfactory. Some errors in the

Table 4 Accuracy results for the Pleiades image using the OBIA classification methods

Classified	Reference						Producer's accuracy (%)	User's accuracy (%)
	Cultivated land	Urban area	Grassland and woods	Water	Coal and coal gangue	Total		
Cultivated land	94	0	7	1	1	103	94	91
Urban area	2	96	0	0	2	100	96	96
Grassland and woods	1	0	92	2	0	95	92	97
Water	1	0	0	97	2	98	97	97
Coal and coal gangue	2	4	1	0	50	59	91	87
Total	100	100	100	100	55	455		
Overall accuracy								94%
Kappa coefficient								0.92

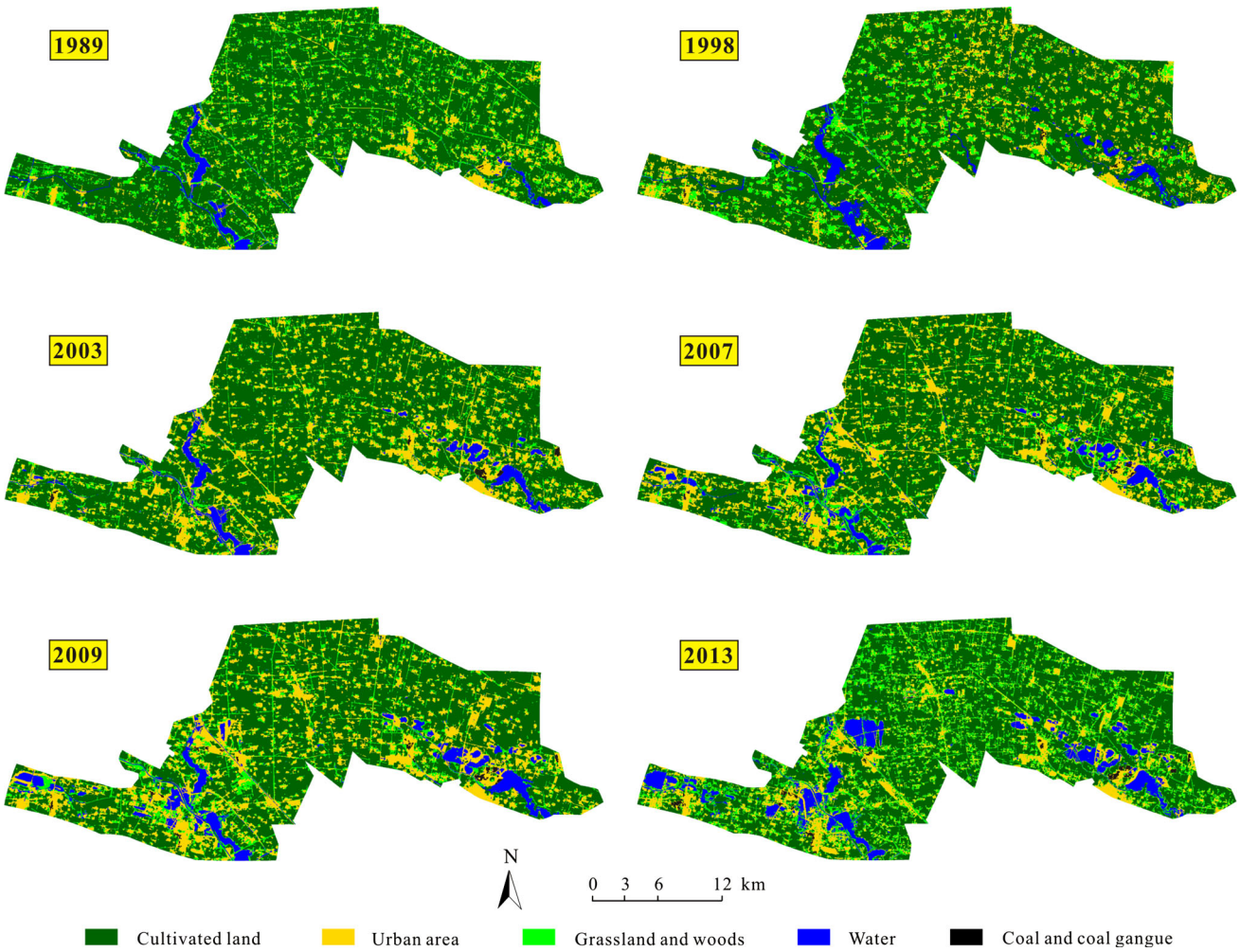

Fig. 6 Land use maps from 1989 to 2013 for the Panxie coal mining area

Table 5 Accuracy results for the Landsat-8 image derived from OBIA classification methods

Classified	Reference						Producer's accuracy (%)	User's accuracy (%)
	Cultivated land	Urban area	Grassland and woods	Water	Coal and coal gangue	Total		
Cultivated land	95	2	13	2	2	114	95	81
Urban area	1	85	0	2	5	93	85	92
Grassland and woods	2	9	86	4	1	102	86	84
Water	0	1	0	89	2	92	89	97
Coal and coal gangue	2	3	1	3	45	54	82	84
Total	100	100	100	100	55	455		
Overall accuracy								88%
Kappa coefficient								0.86

Table 6 Accuracy results of multitemporal classification based on the OBIA classification method

	1989	1998	2003	2007	2009	2013
Overall accuracy (%)	80	82	86	84	85	88
Kappa coefficient	0.75	0.79	0.83	0.81	0.84	0.86

accuracy assessment probably reflect the lack of reliable ground truth data and the mismatch in the timing of the validation satellite images.

Multitemporal Landsat images analyzed to assess land use change using OBIA

The spatial distribution of the five land use classes was extracted to detect land use change in the Panxie coal mining area since the 1980s and to quantitatively analyze the changes based on the OBIA classification from each of the land use maps in the time series (Tables 7, 8). The change matrix analysis showed that, as a whole, about 40% of the land within the study area experienced land use change in one way or another during the 24-year (1989–2013) analysis period. To interpret the land use change results, we used a binary mask of change and no change (Fig. 7). There are some clear spatial patterns of change on the classification maps for the 1989–2013 period. Two of these changes were significant, namely a continuing decline in the area of cultivated land, and a large growth in the urban, coal and coal gangue, and water areas. The study area, as one of the main coal and agricultural production regions in China, was largely dominated by cultivated land in 1989 (73.11% of the total area), and the urban and water areas only occupied 9.38 and 2.77%, respectively. Twenty-four years later, in 2013, the study area was still dominated by cultivated land, but the area had declined by 15.86 percentage points to 57.25%, mainly because of conversion to urban areas (8310 ha), grassland and woods (3232 ha), and water (2899 ha). In contrast, the area of water, which includes tributaries of the Huaihe River and waterlogged areas, increased to roughly three times that covered in 1989, from 2.77 to 7.84%. The increase in the water area was mainly due to the increase in waterlogged areas that have formed since the 1980s because of the underground coal mining activities. More than 50% of the increase in the water area in 2013 came from cultivated land. As with the water area, the area of coal and coal gangue rapidly increased from 10 ha in 1989 to 372 ha in 2013, which represents a 40-fold increase. The areas coal and coal gangue were mainly previously cultivated lands (137 ha), urban areas (128 ha), and grassland and woods (86 ha).

Table 7 Summary of land use classification statistics from 1989 to 2013

Land use types	1989 (%)	1998 (%)	2003 (%)	2007 (%)	2009 (%)	2013 (%)
Cultivated land	73.11	70.34	68.24	64.88	60.08	57.25
Urban area	9.38	12.80	17.93	19.51	21.31	20.92
Grassland and Woods	14.72	12.61	9.33	10.91	11.91	13.41
Water	2.77	4.15	4.33	4.41	6.32	7.84
Coal and coal gangue	0.02	0.1	0.17	0.29	0.38	0.58

Table 8 Summary of the land use change matrix from 1989 to 2013 (unit: ha)

1989	2013					
	Cultivated land	Urban area	Grassland and woods	Water	Coal and coal gangue	Total
Cultivated land	30,643	8310	3232	2899	137	45,221
Urban area	1244	2816	1349	304	128	5831
Grassland and woods	3390	1969	3096	539	86	9080
Water	220	174	442	951	14	1801
Coal and coal gangue	0	2	1	0	7	10
Total	35,497	13,261	8120	4693	372	61,943
Change rate (%)	−21.5	127.4	−10.6	160.6	3620	

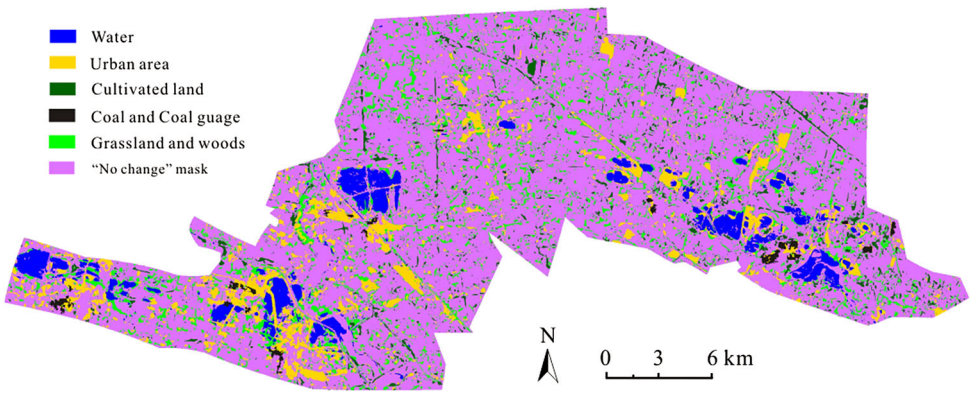

Fig. 7 Land use change from 1989 to 2013

The urban areas first increased to 21.31% in 2009 and then decreased slightly to 20.92% in 2013. The spread in urban land occurred mainly along transport routes and around the coal mining center. Over time, the uneven concentration of urban areas transitioned into a more outwardly dispersed pattern. The urban areas increased mainly at the expense of cultivated land (8310 ha), followed by grassland and woods (1969 ha). Trends in grassland and woods were variable, with an initial decrease to 9.33% in 2003 followed by an increase to 13.41% in 2013. Most of the grassland and woods were distributed around the cultivated land and the residential area or along the rivers and transportation routes.

We carried out an additional accuracy assessments to detect land use change between 1989 and 2013 (Table 9). The accuracy exceeded 85% for both the change and no change mask, which confirms that land use changes in the Panxie coal mining area were accurately detected.

Land use change vs. coal production

We used total coal production data to identify the reasons for land use changes in the Panxie coal mining area. The Huainan Mining Industry (Group) provided information on the total coal production in 1989, 1998, 2003, 2007, 2009, and 2013. Land use classes and growth in mine production are significantly related (Figs. 8, 9). There is a strong positive relationship between coal production and land use classes, especially the 'coal and coal gangue' ($r = 0.99$), 'water' ($r = 0.95$), and 'urban area' ($r = 0.94$) classes, indicating that increases in coal production are correlated with increases in these three classes. On the other hand, there is a strong negative relationship between coal

Table 9 Accuracy assessment of the change mask from 1989 to 2013

		Reference			Accuracy (%)	
		Change	No change	Total	Producer's (%)	User's (%)
Change mask (predicted)	Change	186	33	219	92.54	84.93
	No change	15	221	236	87.01	93.64
	Total	201	254	455		

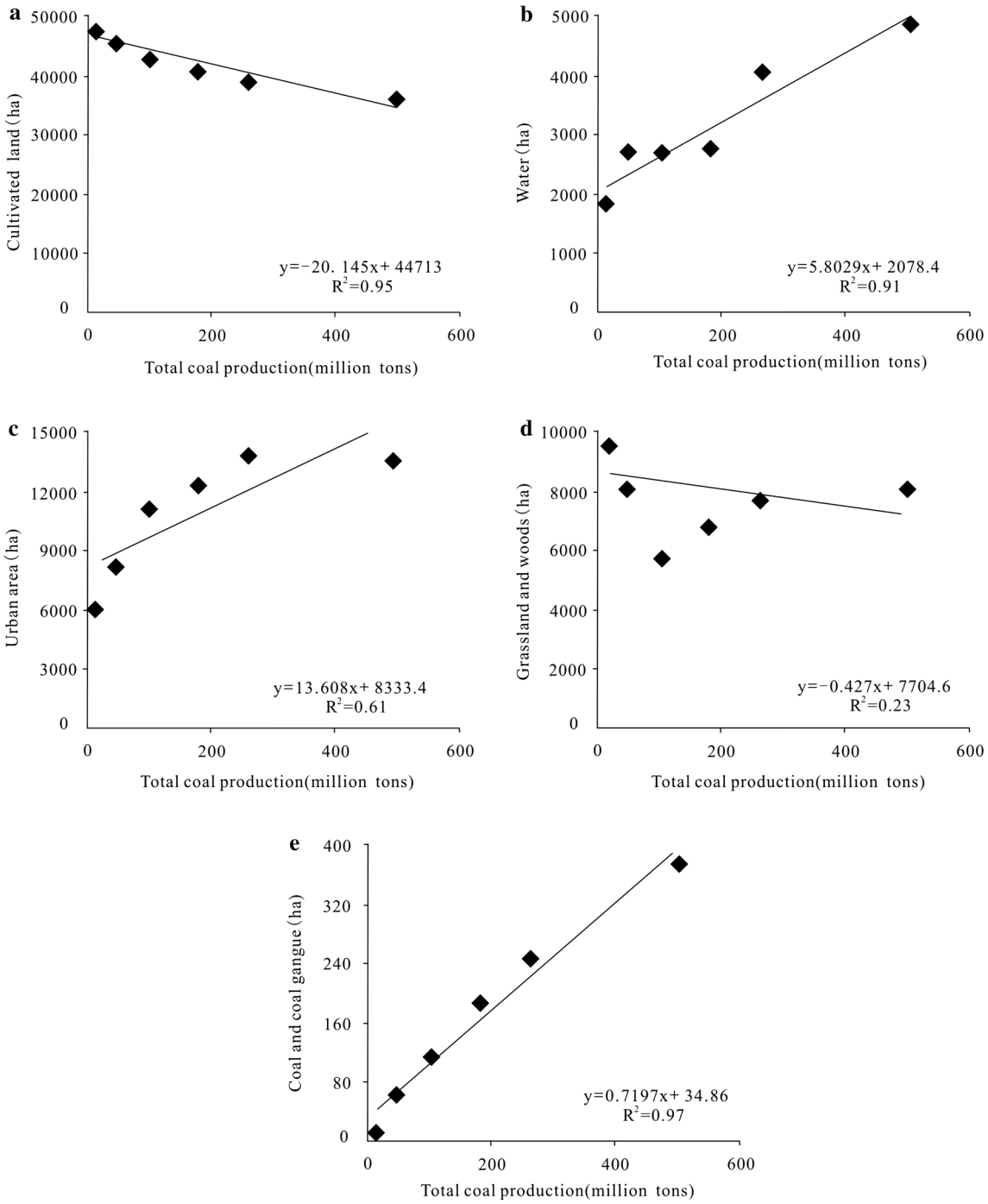

Fig. 8 Relationships between total coal production and areas of **a** cultivated land, **b** water, **c** urban, **d** grassland and woods, and **e** coal and coal gangue

production and the 'cultivated land' class ($r = -0.95$). The ongoing exploitation in the underground coal mines was accompanied by a continual decrease in the area of cultivated land. There is a weak negative relationship between coal production and the 'grassland and woods' class ($r = -0.43$), indicating that this class is not only influenced by underground coal mining activities, but also by urban development, and abandonment of lands. Interconversion occurred between the classes of 'cultivated land' and 'grassland and woods.'

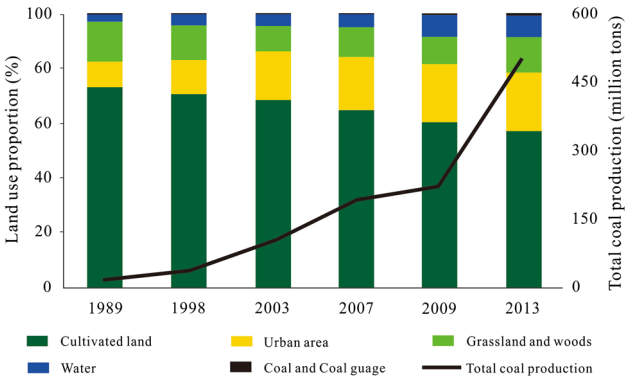

Fig. 9 Proportion of land use classes (*columns*) and total coal production (*line*) from 1989 to 2013

Discussion

We used OBIA to extract land use information and describe dynamic land use change in the Panxie coal mining area from satellite images of different spatial resolutions. The classification results illustrate that the approach is flexible and that the ruleset can be efficiently refined to facilitate the application of this method to land use assessments of other mining regions. The OBIA approach permits many possible combinations of different functions, parameters, features, and variables (Myint et al. 2011). Furthermore, new objects can be selected or modified each time the image is refined until satisfactory results are obtained. In this study, because of the difference between the satellite sensor and the spatial resolution, the threshold values that were used for the high-resolution satellite images (e.g., Pleiades) were not suitable for the medium-resolution satellite images (e.g., Landsat), even though the classification system was based on the same classes in the same study area. The satisfactory classification results obtained from 1989 to 2013 indicate that by slightly modifying the parameters, similar or considerably different threshold values could be useful for mapping the same study area in different periods. The classification accuracy of the Landsat imagery was lower than that for the high-resolution imagery; the objects in the medium-resolution images were sometimes smaller than the spatial resolution of the cells, meaning that some objects were misclassified because of their spectral similarity to other objects (Cleve et al. 2008). Moreover, reference information used for multitemporal classification maps might also affect classification accuracy because of the images from Google Earth, which had some obvious disadvantages, such as low spatial resolution, poor availability and time coherence.

The results of this study indicate that underground coal mining activity has had a profound influence on land use change in the coal mining area (Fig. 9). With a growing demand for coal, particularly in developing countries such as China and India (Wang et al. 2015), these impacts could intensify in the coming decades. An important trend identified in the study area is the expansion of the waterlogged areas (Figs. 6, 7). In 1989, several small waterlogged areas had formed near the Ni River in the southeastern part of the study area. As modern techniques (e.g., heavy equipment) have been introduced to underground coal mining, the waterlogged areas have expanded rapidly. Since 2003, when several new coal mines became operational in the center and west of the Panxie coal mining area, more and more cultivated land and residential areas have become waterlogged, which has meant, depending on the local setting, the loss of livelihoods, a reduced quality of life, and consequent negative impacts on social stability and economic development (Bian et al. 2010). By 2013, the waterlogged areas had expanded to the entire Panxie coal mining area and covered an area of about 2900 ha, which accounted for more than 60% of the total water area in the Panxie coal mining area (Fig. 10). The increased extent of the waterlogged area has affected some tributaries of the Huaihe River and will gradually change the structure of the Huaihe River basin in future decades (Li 2013a, b). These changes will give rise to additional challenges for flood control and the treatment of polluted water, which are already serious problems in the Huaihe River basin.

Increased coal production was matched by an increase in the area of coal gangue heaps. These heaps occupy land and contribute to a reduction in cultivated land and an increase in soil erosion, thereby impacting on the biodiversity of local ecosystems (Sonter et al. 2014a, b). In the Panxie coal mining area, the heaps of coal and coal gangue not only occupy a large amount of land, but may also cause serious contamination of water, soil, and crops (Li 2013a, b; Zhou et al. 2014a, b).

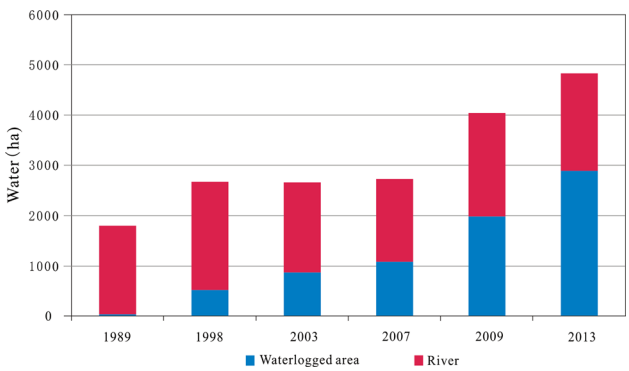

Fig. 10 Proportion of waterlogged areas relative to total water areas from 1989 to 2013

In addition, the dynamic causal relationship between mine expansion and urbanization in the Panxie coal mining area is different from that found for many other cities, where urbanization has generally resulted from normal economic development and population growth. In Panxie, due to modern mining technology and an increase in the number of operational coal mines, urban expansion has shown a unique tendency to spread around the coal mines. Mining and transport infrastructure have increased in proportion with the demands of the mining industry (Figs. 8, 9). Similar trends have been observed in other mining regions in China and worldwide, such as at Xuzhou and Yanzhou, and in the Bowen and Galilee basins in Australia (Du et al. 2007; Hu and Zhao 2007; Petkova-Timmer et al. 2009; Sonter et al. 2014a, b).

It is noteworthy that all of the images selected for this study were acquired in spring (April–May), when vegetation growth is vigorous. Large areas of grassland and woods were distributed around the mining and residential areas. Unfortunately, a small portion of the urban areas below the tree canopy was misclassified as vegetation in 2013 because of city greening initiatives in the preceding years (Li 2013a, b). This misclassification meant that the grassland and woods area was overestimated and the urban areas, which showed a significant reduction when compared with 2009, were underestimated. This explains why the tree canopy feature extraction in urban area has become increasingly important in recent years. The high variation in urban landscapes from the horizontal and vertical planes is one of the major challenges in feature extraction (O'Neil-Dunne et al. 2009). Light detection and ranging (LIDAR) might be able overcome these challenges by providing a wealth of other geospatial information in coal mining areas (Zhou and Troy 2008). A digital surface model (DSM) and a digital elevation model (DEM) can be produced from the LIDAR point cloud to analyze the height and texture of above-ground landscape features. Also, when the images are being segmented and classified, some features or bands cannot be executed at many different scales because of the limitations of computational resources, which need to be sufficiently large to segment huge numbers of objects from many different bands (Myint et al. 2011). This may be a major limitation, especially when processing high-resolution data for a large area.

Conclusions

The OBIA classification method with a set of fuzzy or crisp membership functions was developed so that Pleiades and Landsat images could be used to accurately extract land use information in the Panxie coal mining area. The overall accuracies and Kappa coefficients of all the classification maps were satisfactory. These results suggest that a rule-based reasoning system that combines spectral, texture, and spatial information can quantify the land use classes in images and can significantly improve the classification accuracy in the Panxie coal mining area. This analysis will provide fundamental information for land use classification and land use change analysis. In addition, it may be possible to use the classification rulesets and method described in this paper to extract land use information and detect land use change in other mining regions.

The multitemporal classification results show that between 1989 and 2013, the Panxie coal mining area has experienced rapid and dramatic land use change because of long-term underground coal mining activities. Land use classes and growth in mine production were significantly related. As the mines have expanded, urban, coal and coal gangue, and water areas have also expanded rapidly, causing a corresponding rapid reduction in cultivated land. These observed trends in land use change could be a useful basis for ensure compliance with environmental regulations or permitting in mining regions.

Acknowledgements The research was supported by the National Key Technology R&D Program (No. 2012BAC10B02), the National Natural Science Foundation of China (NSFC: 41372353), and the Huainan Mining Group (No. HNKY-JT-JS-(2013)-004).

References

Baatz M, Schäpe A (2000) Multiresolution segmentation: an optimization approach for high quality multi-scale image segmentation. Beiträge zum AGIT XII:12–23

Belgiu M, Drăguţ L, Strobl J (2014) Quantitative evaluation of variations in rule-based classifications of land cover in urban neighbourhoods using WorldView-2 imagery. ISPRS J Photogramm 87:205–215

Bian Z, Lu Q (2013) Ecological effects analysis of land use change in coal mining area based on ecosystem service valuing: a case study in Jiawang. Environ Earth Sci 68:1619–1630

Bian Z, Zhang Y (2006) Land use changes in Xuzhou coal mining area. Acta Geograph Sin 61:349–358

Bian Z, Inyang HI, Daniels JL, Otto F, Struthers S (2010) Environmental issues from coal mining and their solutions. Min Sci Technol 20:215–223

Blaschke T (2010) Object based image analysis for remote sensing. ISPRS J Photogramm 65:2–16

Blaschke T, Hay GJ, Kelly M, Lang S, Hofmann P (2014) Geographic object-based image analysis-towards a new paradigm. ISPRS J Photogramm 87:180–191

Bunting P, Lucas R (2006) The delineation of tree crowns in Australian mixed species forests using hyperspectral compact airborne spectrographic imager (CASI) data. Remote Sens Environ 101:230–248

Chen Y, Shi P, Fung T, Wang J, Li X (2007) Object-oriented classification for urban land cover mapping with ASTER imagery. Int J Remote Sens 28:4645–4651

Chen X, Zhang ZC, Chen XH, Shi P (2009) The impact of land use and land cover changes on soil moisture and hydraulic

conductivity along the karst hillslopes of southwest China. Environ Earth Sci 59:811–820
Cleve C, Kelly M, Kearns FR, Moritz M (2008) Classification of the wildland–urban interface: a comparison of pixel-and object-based classifications using high-resolution aerial photography. Comput Environ Urban Syst 32:317–326
Desclée B, Bogaert P, Defourny P (2006) Forest change detection by statistical object-based method. Remote Sens Environ 102:1–11
Dong S, Yin H, Yao S, Zhang F (2013) Detecting surface subsidence in coal mining area based on DInSAR technique. J Earth Sci 24:449–456
Du P, Zhang H, Liu P, Tan K, Yin Z (2007) Land use/cover change in mining areas using multi-source remotely sensed imagery. In: IEEE International Workshop on Analysis of Multi-Temporal Remote Sensing images, Leuven, pp 1–7
Espindola GM, Câmara G, Reis IA, Bins LS, Monteiro AM (2006) Parameter selection for region-growing image segmentation algorithms using spatial autocorrelation. Int J Remote Sens 27:3035–3040
Feyisa GL, Meilby H, Fensholt R, Proud SR (2014) Automated water extraction index: a new technique for surface water mapping using Landsat imagery. Remote Sens Environ 140:23–35
Foody GM (2011) Classification accuracy assessment. IEEE Geosci Remote Sens Soc News 1:8–14
Gao B (1996) NDWI—a normalized difference water index for remote sensing of vegetation liquid water from space. Remote Sens Environ 58:257–266
Gao Y, Kerle N, Mas JF (2009) Object-based image analysis for coal fire-related land cover mapping in coal mining areas. Geocarto Int 24:25–36
Haralick RM (1979) Statistical and structural approaches to texture. Proc IEEE 67(5):786–804
Hu Z, Zhao Y (2007) Report of the space-time evolution and countermeasures of the subsidence land reclamation in Yanzhou Coal Mining area. Dissertation, China University of Mining and Technology (Beijing) (**in Chinese**)
Hu Z, Xu X, Zhao Y (2012) Dynamic monitoring of land subsidence in mining area from multi-source remote-sensing data–a case study at Yanzhou, China. Int J Remote Sens 33:5528–5545
Huang X, Lu Q, Zhang L (2014) A multi-index learning approach for classification of high-resolution remotely sensed images over urban areas. ISPRS J Photogramm 90:36–48
Jensen JR (1981) Urban change detection mapping using Landsat digital data. Am Cartograph 8:127–147
Jiao L, Liu Y, Li H (2012) Characterizing land-use classes in remote sensing imagery by shape metrics. ISPRS J Photogramm 72:46–55
Kindu M, Schneider T, Teketay D, Knoke T (2013) Land use/land cover change analysis using object-based classification approach in Munessa–Shashemene landscape of the Ethiopian Highlands. Remote Sens 5:2411–2435
Li JM (2013) Study on flood storage and water logging control in middle course of Huaihe River mining subsidence area. China Institute of Water Resources and Hydropower Research (IWHR)
Li XM (2013b) The city greening in energy city-Huainan. Land Green 7:21 **(in Chinese)**
Lu D, Mausel P, Brondizio E, Moran E (2004) Change detection techniques. Int J Remote Sens 25:2365–2401
Lu D, Hetrick S, Moran E (2011) Impervious surface mapping with QuickBird imagery. Int J Remote Sens 32:2519–2533
Ma X, Liu C (2011) Information extraction of mining-land use based on automatic threshold classification of decision tree. In: 2011 International conference on remote sensing, environment and transportation engineering, pp 421–424
MacFeeters SK (1996) The use of Normalized Difference Water Index (NDWI) in the delineation of open water feature. Int J Remote Sens 17:1425–1432
Moffett KB, Gorelick SM (2013) Distinguishing wetland vegetation and channel features with object-based image segmentation. Int J Remote Sens 34:1332–1354
Myint SW, Gober P, Brazel A, Grossman-Clarke S, Weng Q (2011) Per-pixel vs. object-based classification of urban land cover extraction using high spatial resolution imagery. Remote Sens Environ 115:1145–1161
O'Neil-Dunne J, Pelletier K, Macfaden S, Troy A, Grove JM (2009) Object-based high-resolution land-cover mapping. In: International conference on geoinformatics IEEE pp 1–6
Ouma YO, Tateishi R (2006) A water index for rapid mapping of shoreline changes of five East African Rift Valley lakes: an empirical analysis using Landsat TM and ETM + data. Int J Remote Sens 27:3153–3181
Peneva-Reed E (2014) Understanding land-cover change dynamics of a mangrove ecosystem at the village level in Krabi Province, Thailand, using Landsat data. GISCI Remote Sens 51:403–426
Petkova-Timmer V, Lockie S, Rolfe J, Ivanova G (2009) Mining developments and social impacts on communities: bowen basin case studies. Rural Soci 19:211–228
Prakash A, Gupta RP (1998) Land-use mapping and change detection in a coal mining area-a case study in the Jharia coalfield, India. Int J Remote Sens 19:391–410
Rawashdeh SA, Ruzouq R, Al-Fugara A, Pradhan B, Ziad SH, Ghayda AR (2013) Monitoring of Dead Sea water surface variation using multi-temporal satellite data and GIS. ARAB J Geosci 6:3241–3248
Sheng F, Kuang D (2003) Remote sensing survey and research on the change of Qinghai Lake in recent 25years. Lake Sci 15:289–296 **(in Chinese)**
Shiraishi T, Motohka T, Thapa RB, Watanabe M, Shimada M (2014) Comparative assessment of supervised classifiers for land use—land cover classification in a tropical region using time-series palsar mosaic data. IEEE J Stars 7(4):1186–1199
Sonter LJ, Barrett DJ, Soares-Filho BS, Moran CJ (2014a) Global demand for steel drives extensive land-use change in Brazil's iron quadrangle. Glob Environ Change 26(1):63–72
Sonter LJ, Moran CJ, Barrett DJ, Soares-Filho BS (2014b) Processes of land use change in mining regions. J Clean Prod 84(1):494–501
Stehman SV (2009) Sampling designs for accuracy assessment of land cover. Int J Remote Sens 30(20):5243–5272
Stumpf A, Kerle N (2011) Object-oriented mapping of landslides using Random Forests. Remote Sens Environ 115:2564–2577
Thapa RB, Itoh T, Shimada M, Watanabe M, Takeshi M, Shiraishi T (2014) Evaluation of ALOS PALSAR sensitivity for characterizing natural forest cover in wider tropical areas. Remote Sens Environ 155:32–41
Thenkabail PS, Enclona EA, Ashton MS, Legg C, Dedieu MJ (2004) Hyperion, IKONOS, ALI, and ETM + sensors in the study of African rainforests. Remote Sens Environ 90:23–43
Townsend PA, Helmers DP, Kingdon CC, Mcneil BE, Beurs KM, Eshleman KN (2009) Changes in the extent of surface mining and reclamation in the Central Appalachians detected using a 1976–2006 Landsat time series. Remote Sens Environ 113:62–72
Trimble (2013) eCognition Developer 8.9. User Guide. München: Trimble Germany GmbH
Vitousek PM, Mooney HA, Lubchenco J, Melillo JM (1997) Human domination of Earth's ecosystems. Science 277:494–499
Wang W, Li S, Han J (2015) Analysis of the main global coal resource countries' supply demand structural trend and coal industry outlook. China Min Mag 24(2):5–9 **(in Chinese)**
Wardlow BD, Egbert SL, Kastens JH (2007) Analysis of time-series MODIS 250 m vegetation index data for crop classification in the US Central Great Plains. Remote Sens Environ 108:290–310

Xu H (2006) Modification of normalised difference water index (NDWI) to enhance open water features in remotely sensed imagery. Int J Remote Sens 27:3025–3033

Xu H (2013) Rule-based impervious surface mapping using high spatial resolution imagery. Int J Remote Sens 34:27–44

Yang X, Lo C (2002) Using a time series of satellite imagery to detect land use and land cover changes in the Atlanta, Georgia metropolitan area. Int J Remote Sens 23:1775–1798

Yu J, Zhao H, Wang Y, Xu J (2015) Evaluating land use type change and ecosystem services in Peixian County. Adv Mater Res 1065:2744–2748

Zhao Y (2003) Principles and methods for remote sensing application and analysis. Science Press, Beijing

Zhou W, Troy A (2008) An object-oriented approach for analysing and characterizing urban landscape at the parcel level. Int J Remote Sens 29:3119–3135

Zhou W, Huang G, Troy A, Cadenasso ML (2009) Object-based land cover classification of shaded areas in high spatial resolution imagery of urban areas: a comparison study. Remote Sens Environ 25:53–67

Zhou C, Liu G, Wu D, Fang T, Wang R, Fan X (2014a) Mobility behavior and environmental implications of trace elements associated with coal gangue: a case study at the Huainan coalfield in china. Chemosphere 95:193–199

Zhou W, Cadenasso ML, Schwarz K, Pickett ST (2014b) Quantifying spatial heterogeneity in urban landscapes: integrating visual interpretation and object-based classification. Remote Sens 6:3369–3386